The International Journal of Engineering and Science (IJES)
|| Volume || 7 || Issue || 4 Ver. I || Pages || PP 61-71 || 2018 ||
ISSN (e): 2319 – 1813 ISSN (p): 23-19 – 1805

Experimental Investigation of Turbulence Anisotropy in Free Shear Flows

J. P. Panda, H. V. Warrior
Department of Ocean Engineering and Naval Architecture,
Indian Institute of Technology Kharagpur, Kharagpur 721302, India
Department of Ocean Engineering and Naval Architecture,
Indian Institute of Technology Kharagpur, Kharagpur 721302, India
Corresponding Author: J. P. Panda

----------***ABSTRACT***----------
A passive grid is used in a water tank to produce homogeneous turbulence and decaying grid generated turbulence is studied. An acoustic doppler velocimeter has been used to measure three instantaneous velocity components. The variation of turbulent kinetic energy and Reynolds stress are studied at different locations downstream of the grid. Special attention has been focused on presenting the evolution of Reynolds stress, dissipation and length scale anisotropy tensors at two different grid Reynolds numbers. It is shown that the rate of return to isotropy is different for the three principal directions. The experimental results are used for the assessment of two pressure strain correlations in the studies of the "return to isotropy" of decaying grid generated turbulence.
Keywords *- Grid generated Turbulence, Return to Isotropy, Reynolds Stress, Length Scale.*

Date of Submission: 24-03-2018 Date of Publication: Date: 08-04-2018

I. INTRODUCTION

Turbulence can be generated by using passive or active devices. Passive devices include screens, barriers, grids and spires at the beginning of the water tank / wind tunnel test section (MacPhail [1]). Active device (Poorte and Biesheuvel [2]) include array of air jets combined with barriers and roughness elements. Matika et al. [3] proposed an active device with servo motors rotating its grid rods attached with vens. Larssen and Devenport[4] used such active grids for production of large scale homogeneous turbulence.

Passive devices such as grids mainly consist of bars or rods and can be used for producing turbulence in wind tunnels/ water tanks if the Reynolds number based on the wire diameter is high. Various authors have explored grid turbulence (Uberoi [5], Warhaft [6], Le Penven [7], Comte- Bellot and Corrsin [8], Choi [9]), which has primarily been used as benchmarks for comparing their theoretical predictions with by various turbulence modelers. More recently Hearst and Lavoie [10], Valente and Vassilicos[11], Gomez-Fernandes et al.[12], Hearst and Lavoie [13] and Gomez-Fernandes et al.[14] have studied grid generated turbulence. Zhou et al. [15] have studied the temporal evolution of turbulence generated by regular and multi-fractal grids numerically. Krogstad and Davidson [16] used multi-fractal grids and compared their results with the results of conventionally used grids. In a water tank Murzyn and Belorgey [17] investigated the grid generated turbulence experimentally. Evolution of turbulent Reynolds stresses and integral turbulent length and time scales were studied by Leng and Chanson [18] for free surface flow. Conventionally, grid is located at the entrance of the test section of the wind tunnel/ water tank. Behind the grid, high level of fluctuations is generated due to complicated flow structure resulting from vortices generated at the grid (Ertunc et al. [19]). Finally, the vortices degenerate into turbulent wakes downstream of the grid and their interaction results in turbulence intensification. It is generally assumed that the turbulence so produced is statistically homogeneous 40 to 50 mesh sizes downstream of the grid. After the flow goes along a few mesh sizes, turbulence begins to decay because of the viscous interaction of the energy containing eddies among themselves and with the wall provided there is no other source of turbulence. Near the grid the eddies are large and the eddy size will be reduced to Taylor microscale in the intermediate region and finally to kolmogorov (dissipation) scale and the energy associated with the smallest eddies dissipate as heat. The decay rate is approximately equals to the viscous dissipation rate (Comte- Bellot and Corrsin [8]).

The study of decaying homogenous turbulence has been experimentally observed by many researchers. (Chasnov [20], Choi [9], Nagata et al. [21], Hearst and Lavoie [22], Tucker [23]). Choi and Lumley [24] has studied wind-tunnel turbulence experimentally and explored plane distortion, axisymmetric expansion and

axisymmetric contraction to introduce anisotropies in grid turbulence. They have plotted and evaluated the evolution of Reynolds stress anisotropy in the wind tunnel. Gence and Mathieu [25], Lumley and Newmann [26] have studied the return to isotropy of homogeneous turbulence having been submitted to two successive plane strains. However it is seen that grid-turbulence is generally anisotropic (Grant and Nisbet[27])**.** Djenidi and Tardu [28] had studied the grid generated homogenous turbulence using direct numerical simulations. Anisotropy of the dissipation tensor in a turbulent boundary layer was studied by Antonia [29] through direct numerical simulations, Torrano et al. [30] evaluated the accuracy of eddy viscosity models in the numerical analysis of decaying grid generated turbulence in open wind tunnel. Very few researchers had worked on the evolution of anisotropies near the grid and the corresponding return to isotropy at various grid Reynolds numbers, also there is a need to assess the performance of pressure strain correlations in computational fluid dynamics simulations for decay of grid generated turbulence.

This paper reports an experimental investigation of grid turbulence with the view to investigate exclusively the degree of the anisotropy of the time averaged turbulent field at different grid Reynolds numbers. The results are analyzed with the aim of quantifying the levels of anisotropy and the approach toward isotropy as the turbulence decays along the flow direction. The focus is on the anisotropies of the Reynolds-stress, dissipation and length scale anisotropy tensors. Numerical simulations were also carried out in a computational fluid dynamics code to study the return to isotropy of turbulence using Sarkar and Speziale (Speziale et al. [32], Sarkar and Speziale [33]) and Gibson and Launder [33] pressure strain correlations. The variation of turbulence intensity, turbulent kinetic energy and Reynolds stresses are also studied downstream of the grid.

II. EXPERIMENTAL SET-UP AND DETAILED PROCEDURE

The experiments were conducted in the recirculating water tank at the department of Ocean Engineering and Naval Architecture, IIT Kharagpur. The schematic diagram of the water tank is shown in figure 1a. Side walls of the water tank are made up of glass. The water is recirculated by a pump, its rpm is controlled by an electrical control unit. Without a grid a mean flow velocity of 1 m/s is achievable for a water depth of 0.8 meter. The water tank has width 2 meter and depth 1.5 meter. The grids were placed immediately preceding the test section through a grid holder. The depth of water was 0.8 meter for all the cases of the experiments.

Turbulence was generated by using grids of 2 different mesh sizes. We name the grids as sq20, sq10. The grids are made up of 2.5 cm diameter cylindrical PVC pipes. The mesh length of the grids (M) were taken as 20cm and 10cm respectively. The rigidity of the 2 grids were calculated as 0.23 and 0.43 by using equation (1) as described in Comte-Bellot and Corrsin [8].

$$\sigma = \frac{d_b}{M}(2 - \frac{d_b}{M}) \tag{1}$$

Reynolds number based on the grid mesh size (Nagata et al. [21]) is calculated as

$$\mathrm{Re}_M = \frac{\overline{U}M}{\upsilon} \tag{2}$$

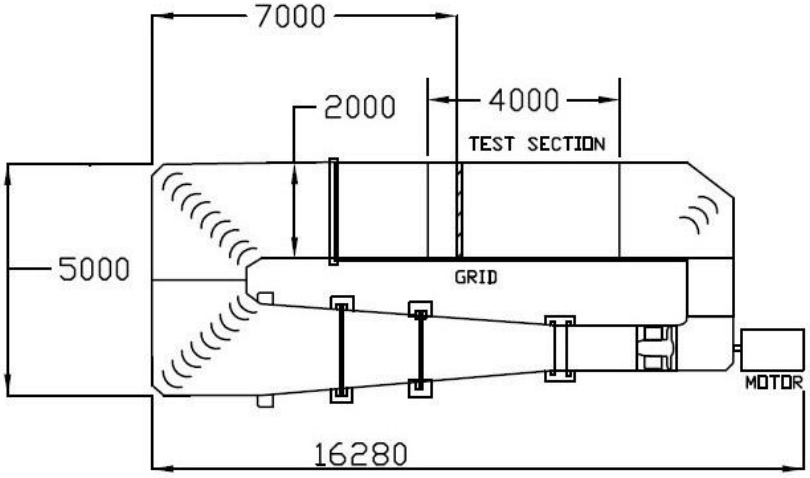

Figure 1: Schematic of the recirculating water tank at the department of Ocean Engineering and Naval Architecture, IIT Kharagpur

Where M is the mesh size, $\overline{U}$ is the inflow velocity and ν is the kinematic viscosity of water. Reynolds numbers corresponding to two different mesh sizes (20 cm, 10 cm) were calculated as Re_M of 80000 and 40000 respectively.

x is the main flow direction (at the grid position, x=0), y is the transverse direction and z is the vertical direction. U, V and W are the horizontal, transverse and vertical velocity components.

An Acoustic doppler velocimeter is used in our experiment to measure instantaneous velocity components at different downstream locations of the grid. Figure 1b represents the adv fitted near the grid in the water tank. An ADV measures three- dimensional flow velocities using doppler shift principle. Main components of the instrument are a sound emitter, three sound receivers and a signal conditioning electronic module. Detailed working principle of operation of the ADV can be found in Gracia et al. [35].

II.1. Data Analysis:

The data collected from the ADV were decomposed into Mean and fluctuating velocities as

$$U = \overline{U} + u' \tag{3}$$

$\overline{U}$ and u' can be calculated from the following formula

$$\overline{U} = \frac{1}{N}\sum_{i=1}^{n} U_i \tag{4}$$

$$u' = \sqrt{\frac{1}{N}(\sum_{i}^{N}(U_i - \overline{U})^2} \tag{5}$$

Since turbulence is considered as eddying motion of fluid, secondary stresses appear in the fluid and those stresses are known as Reynolds stresses, which is a second order tensor having nine components, out of which six are independent. Diagonal components are called as normal stresses and the off diagonal components are called as shear stresses. The turbulent kinetic energy can be defined as

$$k = 0.5(\overline{u'^2} + \overline{v'^2} + \overline{w'^2}) \tag{6}$$

where $\overline{u'^2}$, $\overline{v'^2}$ and $\overline{w'^2}$ are the three normal Reynolds stresses.

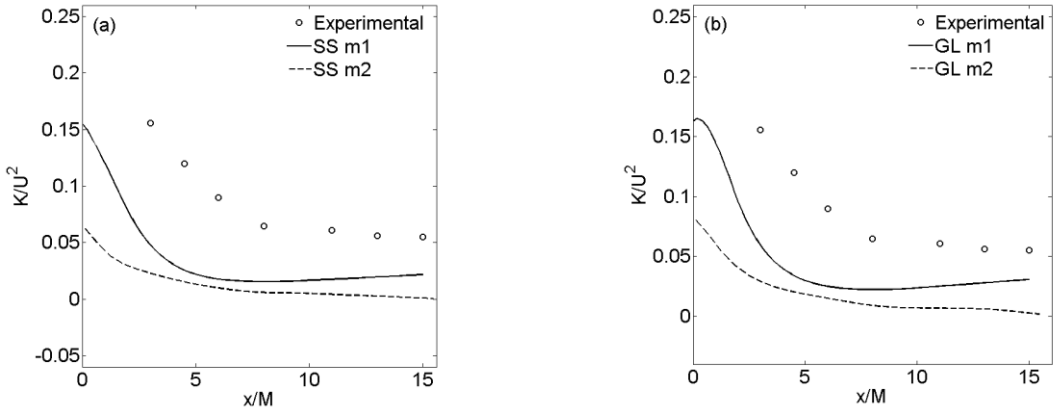

Figure 2: Mesh sensitivity analysis, $\mathrm{Re}_M = 40000$

Flow with a mean velocity gradient is said to be anisotropic. In isotropic turbulence velocity fluctuations are independent of the direction of reference, perfect isotropy condition can be written as

$$\overline{u'^2} = \overline{v'^2} = \overline{w'^2} \tag{7}$$

Anisotropies can exist in Reynolds stress, dissipation and length scale. Various researchers have defined these anisotropies and also have derived relationships among them. Kassinos et al [36] have defined various single point structure tensors which are useful descriptor of turbulence structure. Several one-point statistical measures of the energy-containing turbulence structures were introduced in his seminal work, those are circulicity, inhomogeneity, dimensionality anisotropy tensors.

In this paper main interest will be focused on the downstream evolution of Reynolds stress, dissipation and length scale anisotropy tensors.

II.2. Anisotropy tensors:

Reynolds stress anisotropy:

Reynolds stress anisotropy tensor is defined as (Wilcox [37])

$$b_{ij} = \frac{\overline{u_i u_j} - \frac{2}{3}k\delta_{ij}}{2k} \tag{8}$$

$$II_a = b_{ij}b_{ji} \tag{9}$$

$$III_a = b_{ik}b_{kj}b_{ji} \tag{10}$$

where II_a and III_a are the second and third invariants of the Reynolds stress anisotropy respectively.

Dissipation anisotropy:

Hallback[38] defined the dissipation anisotropy as

$$e_{ij} = k_1 b_{ij} + k_2(b_{ik}b_{kj} - 1/3II_b\delta_{ij}) \tag{11}$$

where $k_1 = k_1(II_b, III_b, \mathrm{Re}_\Lambda, S_2^*, S_3^*, \Omega_2^*)$ and $k_2 = k_2(II_b, III_b, \mathrm{Re}_\Lambda, S_2^*, S_3^*, \Omega_2^*)$

By imposing the zero trace condition $e_{ii} = 0$,symmetry conditions $e_{ij} = e_{ji}$, a general series expansion can be constructed as

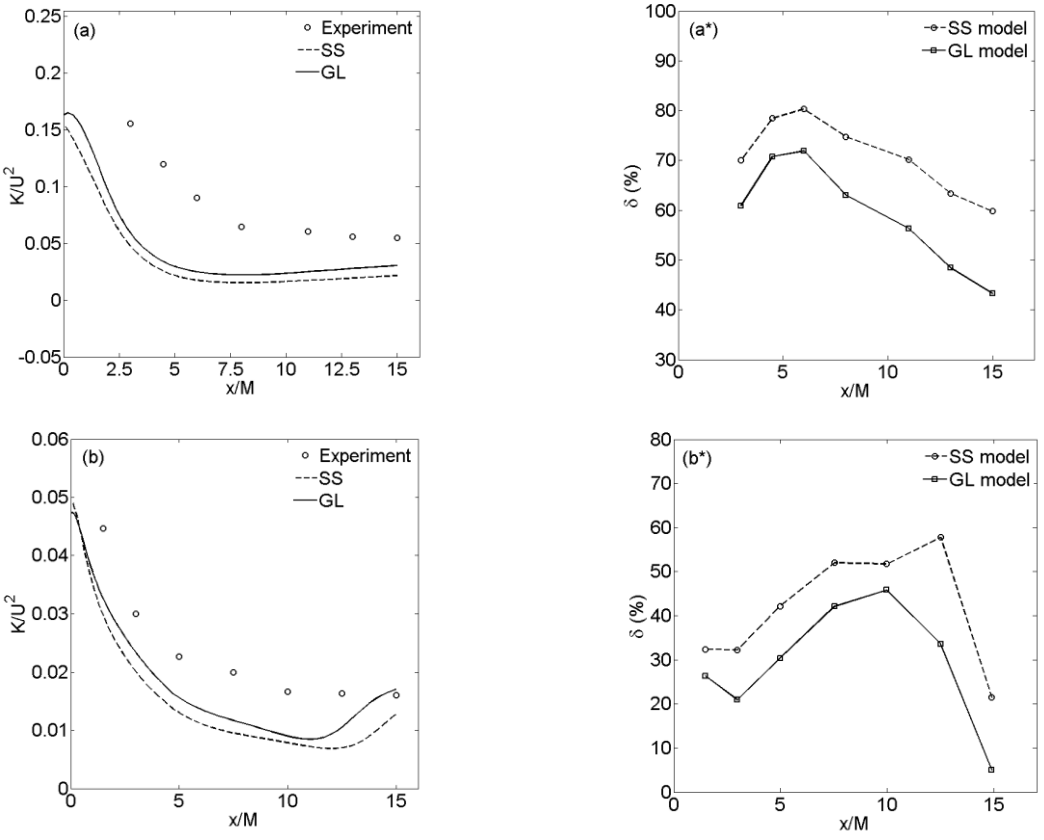

Figure 3: Decay of turbulent kinetic energy a. $\mathrm{Re}_M = 40000$**, b.** $\mathrm{Re}_M = 80000$ **and a*-b* corresponds to the relative errors.**

$$\begin{aligned} e_{ij} &= c_1 b_{ij} + c_2(b_{ik}b_{kj} - 1/3II_b\delta_{ij}) + c_3(b_{ik}b_{kl}b_{lj} - 1/3III_b\delta_{ij}) \\ &+ c_4(b_{ik}b_{kl}b_{lm}b_{mj} - 1/3IV_b\delta_{ij}) + c_5(b_{ik}b_{kl}b_{lm}b_{mn}b_{nj} - 1/3V_b\delta_{ij}) + \ldots \end{aligned} \tag{12}$$

where IV and V are the higher order invariants of Reynolds stress anisotropy. By imposing Cayley- Haminton theorem (Hallback [38]) derived the expression for dissipation anisotropy as

$$e_{ij} = [1 + 0.75(0.5II_b - 2/3)]b_{ij} - 0.75(b_{ik}b_{kj} - 1/3II_b\delta_{ij}) \tag{13}$$

However, Panda et al [31] defined the dissipation anisotropy as

$$e_{ij} = 2k_s b_{ij} \tag{14}$$

where, $k_s = 1 - \sqrt{A}$ (Fu et al. [39])

and k_s is a blending or co-ordinating function.

$$A = 1 - 9/8(II_b - III_b) \tag{15}$$

Using Taylor series, the blending function k_s can be expanded (Warrior et al.[40]) to get

$$k_s = \frac{9}{4}(II_b - 2III_b) \tag{16}$$

Where A is the Lumley's Flatness Parameter (Lumley et al. [41]).

Length scale anisotropy:

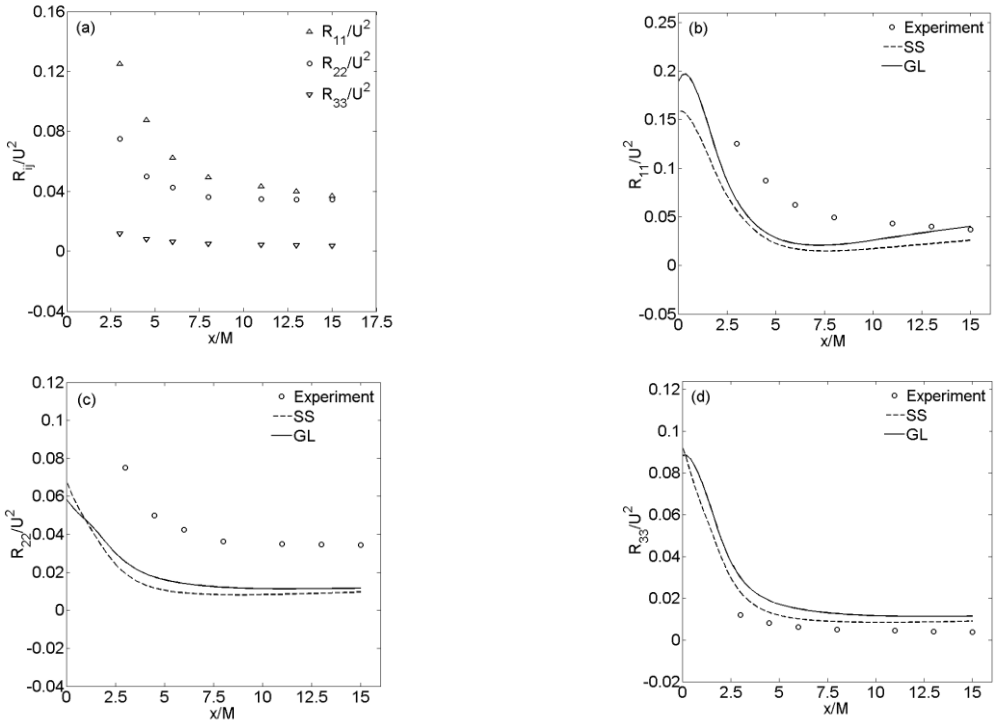

Figure 4: Evolution of Reynolds stresses $\mathrm{Re}_M = 40000$

Basara et al. [42] defined length scale anisotropy in terms Reynolds stress anisotropy and dissipation anisotropy. He defined the Reynolds stress tensor and kinetic energy respectively as

$$\overline{u_i' u_j'} = \lim_{r \to 0} R_{ij}(r,t) \tag{17}$$

$$k = 0.5\overline{u_m' u_m'} \tag{18}$$

The dissipation tensor was also derived as

$$\varepsilon_{ij}(t) = \lim_{r \to 0}[-\upsilon \frac{\partial^2 R_{ij}(r,t)}{\partial r_m \partial r_m}] \tag{19}$$

Finally, the integral length scale tensor was defined as

$$L_{ij}(t) = \frac{3}{8\pi}\frac{1}{k(t)}\int_v \frac{R_{ij}(r,t)}{r^2} dV(r) \tag{20}$$

Cayley-Hamilton theorem was employed to model a relationship between integral length scale tensor, dissipation tensor and Reynolds stress tensor, gives

$$L_{ij}(t) = \frac{3}{4}\frac{k^{3/2}}{\varepsilon}\sum_{m,n=0}^{2} \varphi(m,n)[b_{ik}^m e_{kj}^n + b_{ik}^n e_{kj}^m] \tag{21}$$

Assuming a linear relationship between length scale, dissipation and Reynolds stress tensor Panda et al. [31] adopted a relation between these single point anisotropy tensors

$$l_{ij} = \frac{3}{4}(C_1 b_{ij} + C_2 e_{ij}) \tag{22}$$

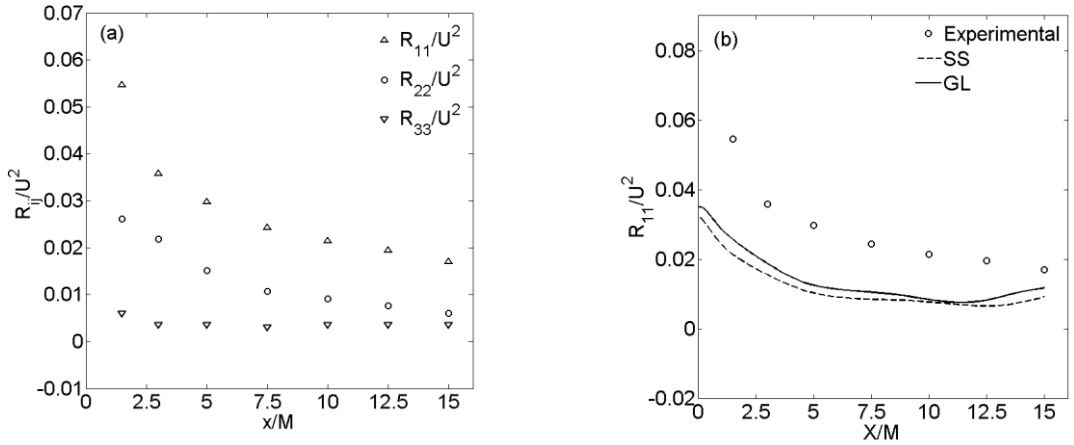

Figure 5: Evolution of Reynolds stresses $\mathrm{Re}_M = 80000$

III. NUMERICAL MODELING AND SIMULATIONS

The mass and momentum conservation equation can be written as

$$\frac{\partial v_i}{\partial x_i} = 0 \tag{23}$$

$$\frac{\partial v_i}{\partial t} + v_j \frac{\partial v_i}{\partial x_j} = -\frac{\partial P}{\partial x_i} + \nu \nabla^2 v_i \tag{24}$$

where u_i is the velocity vector, p is the kinematic pressure, ν is the kinematic viscosity of the fluid. The pressure and velocity can be decomposed into ensemble mean and fluctuating velocities, respectively as:

$v_i = \overline{v_i} + u_i$ and $P = \overline{P} + p$.

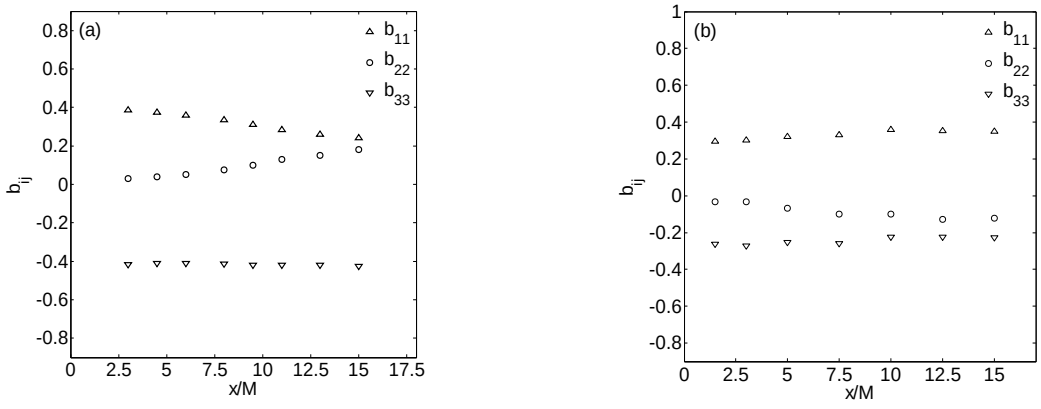

Figure 6: Downstream evolution of Reynolds stress anisotropy at two different grid Reynolds numbers a:40000, b:80000

The Reynolds averaged Navier Stokes equation, which is the evolution equation of the fluctuating velocity, can be derived from equation 23 and 24 as:

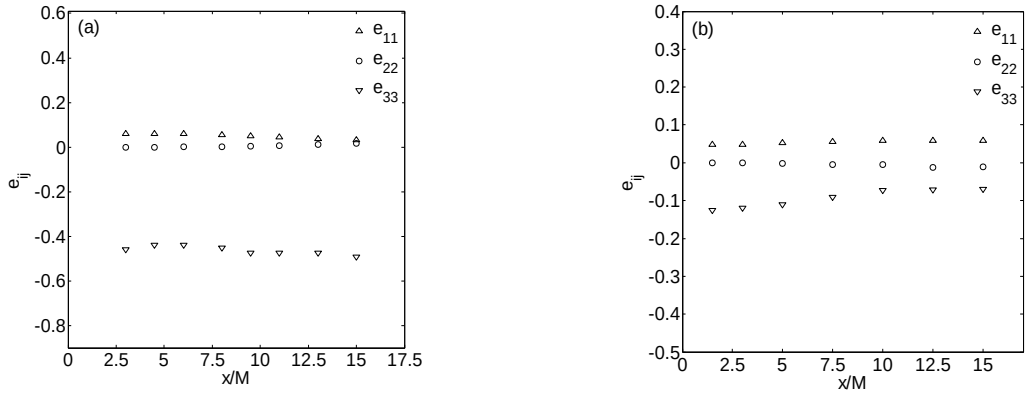

Figure 7: Downstream evolution of dissipation anisotropy

$$\frac{\partial u_i}{\partial t}+\overline{v}_j\frac{\partial u_i}{\partial x_j}=-u_j\frac{\partial u_i}{\partial x_j}-u_j\frac{\partial \overline{v}_i}{\partial x_j}-\frac{\partial p}{\partial x_i}+\partial\nabla^2 u_i+\frac{\partial R_{ij}}{\partial x_j} \tag{25}$$

where $R_{ij}=\overline{u_i u_j}$ is the Reynolds stress tensor.

From above equations, the Reynolds stress transport equation can be derived:

$$\frac{\partial R_{ij}}{\partial t}+U_k\frac{\partial R_{ij}}{\partial x_k}=\mathrm{P}_{ij}+\varepsilon_{ij}-\Pi_{ij}+\frac{\partial}{\partial x_k}[\nu\frac{\partial R_{ij}}{\partial x_k}+C_{ijk}] \tag{26}$$

$$\mathrm{P}_{ij}=-R_{ik}\frac{\partial U_j}{\partial x_k}-R_{jk}\frac{\partial U_i}{\partial x_k} \tag{27}$$

$$\Pi_{ij}=-\frac{1}{\rho}\overline{p(\frac{\partial u_i}{\partial x_j}+\frac{\partial u_j}{\partial x_i})} \tag{28}$$

$$\varepsilon_{ij}=2\nu\overline{\frac{\partial u_i}{\partial x_k}\frac{\partial u_j}{\partial x_k}} \tag{29}$$

$$\rho C_{ijk}=\rho\overline{u_i u_j u_k}+\overline{pu_i}\delta_{jk}+\overline{pu_j}\delta_{ik} \tag{30}$$

where, P_{ij} is denotes the production of turbulence, $T_{ijk,k}$ is the diffusive transport, ε_{ij} is the dissipation rate tensor and Π_{ij} is the pressure strain correlation.

III.1. Analysis of the pressure strain correlations:

The pressure strain correlation of turbulence [43-55] can be separated into two parts

$$\Pi_{ij}=\Pi_{ij}^{s}+\Pi_{ij}^{r} \tag{31}$$

the slow term Π_{ij}^{s} represents turbulence- turbulence interactions and the rapid term Π_{ij}^{r} represents the interaction of turbulence with mean flow gradient i.e. the interaction of eddies with a region of flow with

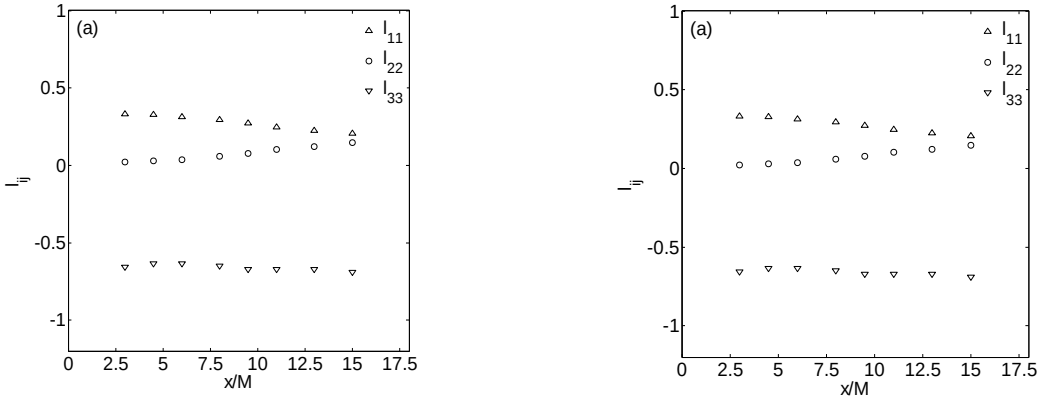

Figure 8: Downstream evolution of length scale anisotropy

different mean velocity. The Poisson equation for fluctuating pressure should be solved for the determination of pressure fluctuations (Mishra and Girimaji [43]), for the modeling of the pressure strain correlation.

$$\frac{1}{\rho}\nabla^2 p = -2\frac{\partial U_i}{\partial x_j}\frac{\partial u_j}{\partial x_i} - \frac{\partial^2}{\partial x_i \partial x_j}(u_i u_j - \overline{u_i u_j}) \tag{32}$$

Equation 32 can be solved through the decomposition of the fluctuating pressure as (Mishra and Girimaji [43])

$$p = p_{slow} + p_{rapid} \tag{33}$$

Slow and rapid pressure fluctuations satisfy the following equations;

$$\frac{1}{\rho}\nabla^2 p_{slow} = -\frac{\partial^2}{\partial x_i \partial x_j}(u_i u_j - \overline{u_i u_j}) \tag{34}$$

$$\frac{1}{\rho}\nabla^2 p_{rapid} = -2\frac{\partial U_i}{\partial x_j}\frac{\partial u_j}{\partial x_i} \tag{35}$$

Mean strain rate has direct effect on rapid pressure fluctuations, since mean velocity gradient appears in equation (35).

III.2. The Pressure Strain Correlations selected to compare the experimental results:
Gibson and Launder (GL) Model:

$$\prod_{ij} = -C_1(\varepsilon / k)(\overline{u_i u_j} - \frac{2}{3}\delta_{ij}k) - C_2(P_{ij} - \frac{2}{3}\delta_{ij}k) \tag{36}$$

where $c_1 = 1.8$ and $c_2 = 0.6$, P is the production of turbulence energy due to the action of mean shear Gibson and Launder [34] .

where $P = -\overline{u_i u_k}\frac{\partial u_i}{\partial x_k}$.

Speziale, Sarkar and Gatski (SSG) Model:

$$\begin{aligned}\Pi_{ij} = &-(C_1\varepsilon + C_1^*\mathrm{P})b_{ij} + C_2\varepsilon(b_{ik}b_{kj} - \frac{1}{3}b_{kl}b_{kl}\delta_{ij}) + (C_3 - C_3^* II^{1/2})K\bar{S}_{ij} + \\ &C_4K(b_{ik}\bar{S}_{jk} + b_{jk}\bar{S}_{ik} - \frac{2}{3}b_{kl}\bar{S}_{kl}\delta_{ij}) + C_5K(b_{ik}\bar{W}_{jk} + b_{jk}\bar{W}_{ik})\end{aligned} \tag{37}$$

The model constants are (Speziale et al. [33])

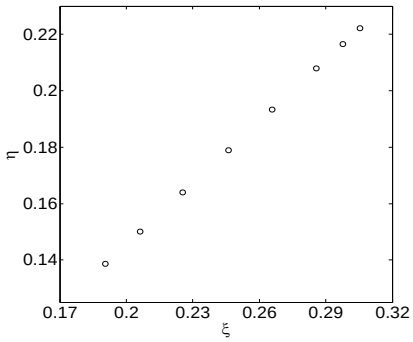

Figure 9: Trajectories of the return to isotropy of decaying homogeneous turbulence in the $\xi-\eta$ coordinates $\mathrm{Re}_M = 40000$

$C_1 = 3.4, C_1^* = 1.8, C_2 = 4.2$

$C_3 = 0.8, C_3^* = 1.3, C_4 = 1.25$

$C_5 = 0.4, C_{\varepsilon 1} = 1.44, C_{\varepsilon 2} = 1.83$

where $\overline{S}_{ij} = 0.5(\frac{\partial \overline{v}_i}{\partial x_j} + \frac{\partial \overline{v}_j}{\partial x_i})$ and $\overline{W}_{ij} = 0.5(\frac{\partial \overline{v}_i}{\partial x_j} - \frac{\partial \overline{v}_j}{\partial x_i})$

III.3. Numerical Method:

In order to study the decaying grid generated turbulence in the water tank, we perform numerical simulations of the physical problem under consideration. The computational domain consists of a virtual three dimensional water tank with grids fixed at a distance of 0.25 meter from the inlet. Complete set of governing equations with different slow pressure strain models are solved by employing a control volume based finite difference method (Patankar [56]). On the water tank inlet and outlet suitable boundary conditions for velocity and pressure were taken. No slip boundary condition is applied at the wall. We employed the line-by-line tridiagonal matrix algorithm to solve the discretized system of linear algebraic equations numerically. Semi-Implict Method for Pressure Linked Equations technique was used to achieve pressure-velocity coupling. Variable sized grid spacing was used, close to the tank walls more densely spaced grids were considered. Within each time step the solution has been iterated to convergence. A strict convergence criterion was taken for the maximum relative errors in all the discretized equations. For our analysis standard thermos-physical properties of water were considered.

IV. RESULTS AND DISCUSSIONS

For mesh sensitivity analysis, two meshes are used in our simulations, Mesh m_1 and m_2 has 1.5 Million and 0.75 Million cells respectively. It is observed from figure 2 that mesh 1 predicts better results for the decay of turbulence kinetic energy, in comparison to mesh 2, so for all the later cases of simulations with our limited computational facility, mesh 1 is used. Figure 3a and 3b represent the decay of turbulent kinetic energy (here after TKE). The TKE decay at $\mathrm{Re}_M = 40000$ is compared to $\mathrm{Re}_M = 80000$, as a function of distance from the grid. The experimental results are compared with model predictions of Sarkar and speziale[25] (hereafter SS) and Gibson- Launder[26] (hereafter GL) slow pressure strain correlations. At both the grid Reynolds numbers the TKE prediction of GL model is better than SS model. The pressure-strain correlation is an indication of the relative distribution of TKE between different components of Reynolds stresses. So it can be said categorically that the redistribution of TKE among different direction components during return to isotropy is better simulated by the GL model for such grid generated turbulence. It is well established that the slow-pressure strain tends to isotropize the fluctuating velocity field and is fairly independent of the mean velocity gradient. Figure 3a* and 3b* represent the relative error associated the model predictions of turbulence kinetic energy. It is calculated by using following formula: $\delta = \left| K_{Sim} - K_{Exp} \right| / K_{Exp}$. From the relative error analysis it is observed that %age error is more for lower grid Reynolds Number and it is noticed that for $\mathrm{Re}_M = 40000$, error is maximum near the grid. This could be because the magnitude of TKE is more at the grid for both Reynolds numbers.

In Figure 4,5 Reynolds stresses are plotted against non-dimensional downstream distance. The return to isotropy behavior among the components of the Reynolds stresses is not same. GL model prediction of R_{11} and R_{22} is better than SS model. It may be noted that the SS model has some problems, especially in the near-wall region. This is mainly due to the insufficiency of the parameterization of pressure-strain correlation due to wall effects. Thus, it is important that we get the relation between the pressure-strain correlation and the anisotropy tensor correctly as has been attempted in Warrior et.al [40].

The development of principal values of Reynolds stress anisotropy tensor is given in figure 6. These graphs represent the degree of anisotropy in each principal direction. At two different grid Reynolds numbers it was observed that the rate of return to isotropy is not same and also energy transfer pattern among the components of Reynolds stress anisotropy is different. Because of wall and free surface effects (here after fse) the return to isotropy behavior for different grid Reynolds number is different along the three principal directions. This proves that return to isotropy is highly nonlinear process. Figures 7 and 8 shows the evolution of dissipation and length scale anisotropy at different Reynolds numbers respectively.

Trajectories of return to isotropy in ξ and η phase space are plotted in figure 9 at grid Reynolds number 40000. Here, Figure 9 is a phase space portrait (η–ξ) graph, where $\eta = II_b^{1/2}$ and $\xi = III_b^{1/3}$. Rotta assumed a straight line in phase space. SSG assumes a curved quadratic model. It is evident from Figure 9 that the present experiment has generated results that are consistent with these two schemes. There seems to be some curvature due to non-linearity, but it is quite small.

V. CONCLUSION

In this paper, an acoustic doppler velocimeter was used to measure velocity fields, the evolution of anisotropic tensors, kinetic energy and Reynolds stresses downstream of two grids sq10 and sq20 were studied in the flow field. We found that with increase in grid Reynolds number turbulence kinetic energy level decreases past the grid, i.e. smaller is the grid size, TKE of the flow is more past the grid. Decay of the turbulence kinetic energy is mainly concentrated closed the grid (x/M<15) and in sq10 we observed faster decay of turbulence kinetic energy. It was also found that the rate of return to isotropy is different for the three principal directions for different grid Reynolds numbers. We observed that the GL model predictions of Reynolds stress distributions are better in comparison to the SS model. Experimental data presented in this paper can be used for development and calibration of turbulence models for highly anisotropic free shear flows.

REFERENCES

[1]. MacPhail, D. C, " An Experimental Verification of the Isotropy of Turbulence Produced by a Grid, " Journal of the Aeronautical Sciences, Vol. 8, No. 2, pp. 73-75, December, 1940.

[2]. Poorte R. E. G. and Biesheuvel A., 2002, "Experiments on the motion of gas bubbles in turbulence generated by an active grid," J. Fluid Mech. 461, 127–154.

[3]. Makita H, 1991, " Realization of a large-scale turbulence field in a small wind tunnel, " Fluid Dyn Res 8:53–64.

[4]. Larssen, J. V. & Devenport, W. J. 2011, "On the generation of large-scale homogeneous turbulence, "Exp. Fluids 50, 1207–1223.

[5]. Uberoi, M. S. 1956, "Effect of wind-tunnel contraction on free-stream turbulence, " J. Aero. Sci. 23, 754.

[6]. Warhaft, Z., and Lumley, J. L., 1978, "An Experimental Study of the Decay of Temperature Fluctuations in Grid-Generated Turbulence," J. Fluid Mech., 88(4), pp. 659–684.

[7]. Le Penven, L., Gence, J. N. & Comte-Bellot, G. 1985, "On the approach to isotropy of homogeneous turbulence: Effect of partition of kinetic energy among the velocity components, " In Frontiers in Fluid Mechanics (ed. S. H. Davis & J. L. Lumley), pp. 1–21. Springer.

[8]. Comte-Bellot, G. & Corrsin, S. 1966, "The use of a contraction to improve the isotropy of grid-generated turbulence, " J. Fluid Mech. 25, 657.

[9]. Choi, K.-S. 1983 A study of the return to isotropy of homogeneous turbulence. PhD thesis, Cornell University.

[10]. R. J. Hearst and P. Lavoie, 2014 "Scale-by-scale energy budget in fractal element grid-generated turbulence," J. Turbul. 15, 540.

[11]. P. C. Valente and J. C. Vassilicos, 2011, "The decay of turbulence generated by a class of multiscale grids," J. Fluid Mech. 687, 300.

[12]. R. Gomes-Fernandes, B. Ganapathisubramani, and J. C. Vassilicos, 2012, "Particle image velocimetry study of fractal-generated turbulence," J. Fluid Mech. 711, 306.

[13]. R. J. Hearst and P. Lavoie, 2015, "Velocity derivative skewness in fractal generated, non-equilibrium grid turbulence," Phys. Fluids 27, 071701.

[14]. R. Gomes-Fernandes, B. Ganapathisubramani, and J. C. Vassilicos, 2015, "The energy cascade in near-field non-homogeneous non-isotropic turbulence," J. Fluid Mech. 771, 676.

[15]. Y. Zhou, K. Nagata, Y. Sakai, H. Suzuki, Y. Ito, O. Terashima, and T. Hayase,2014, "Relevance of turbulence behind the single square grid to turbulence generated by regular- and multiscale-grids," Phys. Fluids 26, 075105.

[16]. Krogstad, P.A. & Davidson, P. A. 2011," Free decaying, homogeneous turbulence generated by multi-scale grids. J. Fluid Mech. 680, 417–434.

[17]. Murzyn, F., and Belorgey, M., 2005, "Experimental Investigation of the Grid Generated Turbulence Features in a Free Surface Flow," Exp. Therm. Fluid Sci., 29(8), pp. 925–935.

[18]. Leng, X., and Chanson, H., 2017, "Integral turbulent scales in unsteady rapidly varied open channel flows," Exp. Therm. Fluid Sci., 81, pp. 382–395.
[19]. Ertunc, L., Ozyilmaz, N., Lienhart, H., Durst, F. & Beronov, K. 2010 Homogeneity of turbulence generated by static-grid structures. J. Fluid Mech. 654, 473–500.
[20]. Chasnov, J. R. 1995 The decay of axisymmetric homogeneous turbulence. Phys. Fluids 7, 600–605.
[21]. Nagata, K., Saiki K., Sakai, Y., Ito, Y., Iwano, K., 2017, "Effect of grid geometry on non-equilibrium dissipation in grid turbulence". Phys. Fluids 29, 015102.
[22]. Hearst, R. J., and Lavoie, P., 2016, "Effects of multi-scale and regular grid geometries on decaying turbulence," J. Fluid Mech., vol. 803, pp. 528-555.
[23]. Tucker, H. J. 1970 The distortion of turbulence by irrotational strain. PhD thesis, McGill University.
[24]. Choi, K.–S., and Lumley, J. L., 2001, "The Return to Isotropy of Homogeneous Turbulence," J. Fluid Mech., 436, pp. 59–84.
[25]. Gence, J. N. & Mathieu, J. 1980, "The return to isotropy of an homogeneous turbulence having been submitted to two successive plane strains". J. Fluid Mech. 101, 555.
[26]. Lumley, J. L. & Newman, G. R. ,1977, " The return to isotropy of homogeneous turbulence". J. Fluid Mech. 82, 161.
[27]. Grant, H. L. & Nisbet, I. C. T ,1957, "The inhomogeneity of grid turbulence". J. Fluid Mech. 2, 263–272.
[28]. L. Djenidi and S. Tardu, "On the anisotropy of a low -Reynolds number grid turbulence," J. Fluid Mech. 702, 332 (2012).
[29]. Antonia, R. A., Djenidi, L. & Spalart, P. R. ,1994, "Anisotropy of the dissipation tensor in a turbulent boundary layer ". Phys. Fluids 6, 2475–2479.
[30]. Torrano, Ivan, Mustafa Tutar, Manex Martinez-Agirre, Anthony Rouquier, Nicolas Mordant, and Mickael Bourgoin. 2015. "Comparison of Experimental and RANS based Numerical Studies of the Decay of Grid-Generated Turbulence." Journal of Fluids Engineering 137 (6): 061203.
[31]. Panda J.P., Warrior, H. V., Maity, S., Mitra A., Sasmal, K., 2017, An improved model including length scale anisotropy for the pressure strain correlation of turbulence", ASME Journal of Fluids Engineering, Vol. 139 / 044503-1.
[32]. Speziale, C. G., Sarkar, S., and Gatski, T. B., 1991, "Modelling the Pressure-Strain Correlation of Turbulence: An Invariant Dynamical Systems Approach," J. Fluid Mech., 227, pp. 245–272.
[33]. Sarkar, S., and Speziale, C., 1990, "A Simple Non-Linear Model for Return to Isotropy in Turbulence" Phys. Fluids A, 2, pp. 84–93.
[34]. M.M. Gibson, B.E. Launder, 1978 "Ground effects on pressure fluctuations in the atmospheric boundary layer", J. Fluid Mech. 86, pp.491–511.
[35]. Garcia, C. M., Cantero, M. I., Nino, Y., and Garcia, M. H. (2005). "Turbulence measurements with acoustic Doppler velocimeters." J. Hydraul. Eng., 10.1061/(ASCE)0733-9429(2005)131:12(1062), 1062–1073.
[36]. Kassinos, Stavros C., William C. Reynolds, and Mike M. Rogers., 2001, "One-point turbulence structure tensors."Journal of Fluid Mechanics 428, 213-248.
[37]. Wilcox, D.C., 1998, Turbulence modeling for CFD. 2nd edn. DCW Indus., La Cañada, CA.
[38]. Hallback, M., Groth J., Johansson A., 1990, "An algebraic model for nonisotropic turbulent dissipation rate in Reynolds stress closures" Phys. Fluids A 2 (10), 0899-8213.
[39]. Fu, S, Launder, B.E and Tselepidakis, D.P., 1987, Accomodating the effects of high strain rates in modeling the pressure-strain correlation, UMIST Mech. Eng. Dept. Report TFD/87/5.
[40]. Warrior, H. V., Mathews, S.,Maity, S. , Sasmal, K., 2014, " An Improved Model for the Return to Isotropy of Homogeneous Turbulence" , ASME Journal of Fluids Engineering, Vol. 136 / 034501-1.
[41]. Lumley, J. L. 1978 Computational modelling of turbulent flows. In Advances in Applied Mechanics, vol. 18, pp. 123–175. Academic.
[42]. Basara, B., and Younis, B. A., 1995, "Prediction of Turbulent Flows in Dredged Trenches," J. Hydraul. Res., 33, pp. 813–824.
[43]. Mishra, A., Girimaji, S., 2017, "Toward approximating non-local dynamics in single-point Pressure-strain correlation closures."Journal of Fluid Mechanics, vol. 811, pp. 168-188.
[44]. Mishra, A. A., and Girimaji, S. S., 2013. "Intercomponent energy transfer in incompressible homogeneous turbulence: multi-point physics and amenability to one-point closures". Journal of Fluid Mechanics, 731, pp. 639–681.
[45]. Mishra, A. A., and Girimaji, S. S., 2010. "Pressure–strain correlation modeling: towards achieving consistency with rapid distortion theory". Flow, turbulence and combustion, 85(3-4), pp. 593–619.
[46]. Mishra, A. A., 2014. "The art and science in modeling the pressure-velocity interactions". PhD Thesis, Texas A&M University, College Station, TX, August.
[47]. Panda J.P., Warrior, H. V. 2018, A representation theory based model for the rapid pressure strain correlation of turbulence", ASME Journal of Fluids Engineering, Vol. 140 / 081101-1.
[48]. Panda, J., Warrior, H., 2017. A pressure strain correlation model employing extended tensor bases. arXiv preprint arXiv: 1712.08005.
[49]. Panda, J., Warrior, H., 2017. Pressure strain correlation modeling for turbulent flows. arXiv preprint arXiv: 1803.02031.
[50]. Maity S, Warrior H (2011) Reynolds stress anisotropy based turbulent eddy viscosity model applied to numerical ocean models. J Fluids Eng 133:064501.
[51]. Sasmal, K., Maity, S. & Warrior, H.V. Ocean Dynamics (2015) 65: 969. https://doi.org/10.1007/s10236-015-0852-8.
[52]. Sasmal K, Maity S, Warrior HV (2014) On the application of a new formulation of nonlinear eddy viscosity based on anisotropy to numerical ocean models. J Turbul 15(8):516–539.
[53]. Mishra, A., & Girimaji, S. (2014). On the realizability of pressure–strain closures. *Journal of Fluid Mechanics, 755*, 535-560. doi:10.1017/jfm.2014.446.
[54]. A. A. Mishra and S. S. Girimaji, Manufactured turbulence with Langevin Equations, ERCOFTAC Bull. 92, 11 (2012).
[55]. S. S. Girimaji, 2000, ''Pressure-strain correlation modeling of complex turbulent flows,'' J. Fluid Mech. 422, 91.
[56]. Patankar, S.V., 1980, Numerical Heat Transfer and Fluid Flow. Hemisphere Publishing Corporation, Taylor and Francis Group, New York.

J. P. Panda ." Experimental Investigation of Turbulence Anisotropy in Free Shear Flows" The International Journal of Engineering and Science (IJES) 7.4 (2018): 61-71